Published in final edited form as:
ACS Nano. 2013 March 26; 7(3): 2068–2077. doi:10.1021/nn304332s.

A Comparison Study of Gold Nanohexapods, Nanorods, and Nanocages for Photothermal Cancer Treatment

Yucai Wang[†,⊥,€], **Kvar C. L. Black**[‡,⊥], **Hannah Luehmann**[‡], **Weiyang Li**[†], **Yu Zhang**[†,€], **Xin Cai**[†], **Dehui Wan**[†], **Si-Yun Liu**[§], **Max Li**[†], **Paul Kim**[†], **Zhi-Yuan Li**[§], **Lihong V. Wang**[†], **Yongjian Liu**[‡,*], and **Younan Xia**[†,€,*]

[†]Department of Biomedical Engineering, Washington University, St. Louis, Missouri 63130, United States

[‡]Department of Radiology, Washington University School of Medicine, St. Louis, Missouri 63110, United States

[§]Laboratory of Optical Physics, Institute of Physics, Chinese Academy of Sciences, Beijing 100190, China

Abstract

Gold nanohexapods represent a novel class of optically tunable nanostructures consisting of an octahedral core and six arms grown on its vertices. By controlling the length of the arms, their localized surface plasmon resonance peaks could be tuned from the visible to the near-infrared region for deep penetration of light into soft tissues. Herein we compare the *in vitro* and *in vivo* capabilities of Au nanohexapods as photothermal transducers for theranostic applications by benchmarking against those of Au nanorods and nanocages. While all these Au nanostructures could absorb and convert near-infrared light into heat, Au nanohexapods exhibited the highest cellular uptake and the lowest cytotoxicity *in vitro* for both the as-prepared and PEGylated nanostructures. *In vivo* pharmacokinetic studies showed that the PEGylated Au nanohexapods had significant blood circulation and tumor accumulation in a mouse breast cancer model. Following photothermal treatment, substantial heat was produced *in situ* and the tumor metabolism was greatly reduced for all these Au nanostructures, as determined with ^{18}F-flourodeoxyglucose positron emission tomography/computed tomography (^{18}F-FDG PET/CT). Combined together, we can conclude that Au nanohexapods are promising candidates for cancer theranostics in terms of both photothermal destruction and contrast-enhanced diagnosis.

Keywords

theranostics; gold nanostructures; near-infrared; photothermal effect; tumor ablation

Photothermal treatment, also known as photothermal ablation or optical hyperthermia, has been actively explored as a minimally invasive approach to cancer therapy.[1] It is a procedure based on localized heating due to light absorption for selective destruction of abnormal cells. In general, near-infrared (NIR, 700–1100 nm) light is preferred for such an application as it can penetrate soft tissues deeply owing to the relatively low absorption/scattering by

[*]Address correspondence to younan.xia@bme.gatech.edu; liuyo@mir.wustl.edu.
[⊥]These authors contribute equally to this work
[€]Present address: The Wallace H. Coulter Department of Biomedical Engineering, Georgia Institute of Technology and Emory University, Atlanta, Georgia 30332, United States

Supporting Information Available: additional figures and information as described in the text. This material is available free of charge *via* the Internet at http://pubs.acs.org.

hemoglobin and water in this so-called transparent window.[2,3] The key component of this technique is a photothermal transducer that can absorb and convert NIR light into heat through a non-radiative mechanism with high efficiency.[4,5]

Over the past decade, many different types of photothermal transducers have been reported, including organic compounds or materials (*e.g.,* indocyanine green (ICG)[6] and polyaniline[7]), metal nanostructures (*e.g.,* Au nanostructures[8] and Pd nanoplates[9]), and carbon-based materials (*e.g.,* carbon nanotubes[10,11] and graphene oxide[12,13]). When combined with NIR light, all of them were able to generate sufficient heat to raise the local temperature and thus kill cancer cells. Of these photothermal transducers, Au nanostructures have received great interest in recent years due to the fact that their localized surface plasmon resonance (LSPR) peaks can be easily tuned to the NIR region by altering their size, shape, structure, or a combination of these parameters.[14] A wide variety of Au nanostructures, including aggregates of colloidal particles,[15] nanoshells,[16] nanocages,[17] nanorods,[18] and nanocrosses[19] have been demonstrated for photothermal cancer therapy with NIR light. In general, the nanostructures should have the following features: *i*) large absorption cross-sections in the NIR region; *ii*) easy functionalization with a "stealth" coating together with targeting ligands to maximize their accumulation at the tumor site following systemic administration; *iii*) appropriate size range (10–100 nm) to increase their blood half-life and to reduce removal by the reticuloendothelial system (RES); and *iv*) good biocompatibility especially in considering the possible long-term *in vivo* presence of the nanostructures.[20] Photothermal therapy has been demonstrated with certain types of Au nanostructures in early clinical trials. As an example, pilot clinical studies with AuroShell® (Au nanoshells with about 150 nm in diameter with a coating of polyethylene glycol 5000) have been approved by FDA and given intravenously to patients for the treatment of head and neck cancer, as well as primary and/or metastaic lung tumors.[21,22] However, developing Au nanostructures with all the aforementioned features remains to be achieved. For Au nanoshells, they are typically more than 100 nm in diameter and tended to be removed by the RES, primarily the liver and spleen.[22] As for Au nanorods, the cetyltrimethylammonium bromide (CTAB) used as a surfactant stabilizer for the synthesis could cause cytotoxicity and thus needs to be replaced prior to any *in vitro* or *in vivo* application.[23]

Branched or star-shaped Au nanostructures consisting of a core and protruding arms have recently received particular interest due to their unique morphology and optical properties.[24–27] Owing to the presence of sharp tips as well as their high surface-to-volume ratios, branched Au nanostructures could be more effective in photothermal conversion and drug loading relative to those with smooth surfaces.[27] We recently reported a new class of branched Au nanostructures -- Au nanohexapods, which consist of an octahedral core and six arms grown on its six vertices.[28] By controlling the length of the arms, the LSPR peaks of the Au nanohexapods could be easily tuned from the visible to the NIR region.[28] Therefore, Au nanohexapods are potential candidates as photothermal transducers for various theranostic applications.

Herein we assessed the potential use of Au nanohexapods as photothermal transducers by benchmarking against Au nanorods and nanocages. We found that Au nanohexapods exhibited a comparable photothermal efficiency, higher cell uptake, and lower cell cytotoxicity relative to Au nanorods and Au nanocages. More importantly, the *in vivo* photothermal treatment studies with a MDA-MB-435 breast cancer model showed that Au nanohexapods were also effective for photothermal destruction of tumor, following either intravenous or intratumoral administration.

RESULTS AND DISCUSSION

Preparation and Characterization of Au Nanostructures

The Au nanohexapods, consisting of an octahedral core and six arms grown on its six vertices, were prepared by reducing $HAuCl_4$ with DMF in an aqueous solution containing Au octahedral seeds using a previously published protocol.[28] By controlling the length of the arms, the longitudinal LSPR peak was tuned to 805 nm (Figure 1A) to overlap with the central wavelength of the diode laser (808 nm). In addition, a second peak was observed at 540 nm in the UV-vis spectrum, which could be attributed to the LSPR of the central octahedral core.[29] The surface of the as-prepared nanohexapods was covered by poly(vinyl pyrrolidone) (PVP, Mw ≈ 55,000), a biocompatible polymer. Figure 1B shows a typical TEM image of the nanohexapods, where the edge length of the octahedral cores was 25.3 ± 0.9 nm and the average dimensions of the arms were 16.3 ± 2.2 nm in length and 13.6 ± 1.8 nm in width, respectively. We measured the extinction coefficients of the Au nanohexapods by using inductively coupled plasma mass spectrometer (ICP-MS) analysis to quantitatively determine the concentration of Au nanohexapods in an aqueous suspension (see Supporting Information for how to calculate the volume of a Au nanohexapod), and then combined it with the extinction measured using a conventional UV-vis spectrometer to obtain a molar extinction coefficient of 5.5×109 M^{-1} cm^{-1} at the longitudinal LSPR peak position (805 nm). We then used a method based on photoacoustic (PA) imaging (λ=800 nm) to measure the molar absorption coefficient of the Au nanohexapods.[30] In this case, the PA signal intensities from suspensions of Au nanohexapods of various particle concentrations were plotted as a function of concentration. As shown in Figure S1, the PA signal increased linearly as the particle concentration was increased. The absorption coefficient of Au nanohexapods was then obtained by benchmarking the PA signal against a linear calibration curve obtained from a set of indocyanine green (ICG) solutions with different concentrations by using the molar absorption coefficient reported for ICG at λ=800 nm (Figure S2).[31] The molar absorption coefficient of the Au nanohexapods was found to be 5.0×109 M^{-1} cm^{-1}, together with a ratio of absorption to extinction coefficients being 0.91. The large absorption cross section of Au nanohexapods indicated that these highly branched structures were effective in absorbing rather than scattering the incident light, suggesting their use as photothermal transducers for theranostic applications.

The widely investigated photothermal transducers, Au nanocages and Au nanorods, were chosen as benchmarks for a comparative study. Their LSPR peaks were also tuned to match the central wavelength of the laser diode (808 nm). The preparation of Au nanorods was performed using a seed-mediated growth method in the presence of the shape-directing surfactant CTAB as described in literature.[32, 33] The as-prepared Au nanorods had an LSPR peak at 800 nm (Figure 1C), and an average length and width of 36.2 ± 2.3 and 9.1 ± 1.7 nm, respectively (Figure 1D). Their surfaces were covered by CTAB. As for Au nanocages, they were prepared using a galvanic replacement reaction between Ag nanocubes and $HAuCl_4$ according to our published protocol.[34] The as-prepared Au nanocages had an LSPR peak at 802 nm (Figure 1E), an outer edge length of 47.4 ± 4.5 nm and an inner edge length of 37.1 ± 2.7 nm, and a wall thickness of 5.2 nm (Figure 1F) and. Their surfaces were covered by PVP.

We also used the discrete dipole approximation (DDA) method to calculate the extinction cross section (σ_{ext}) of Au nanohexapods at various orientations and found several plasmon resonance peaks from 700 nm to 900 nm in addition to the resonance peak at 525 nm (Figure S3). The peak positions were in reasonable agreement with the experimentally measured values (Figure 1A). The appearance of only one relatively broad NIR peak in the measured UV-vis spectrum was likely caused by the random orientations of the particles in the solution and the polydispersity of the sample. Figure S3 also shows the scattering cross

section (σ_{sca}) computed for a Au nanohexapod, and its absorption cross section (σ_{ext}, data not shown) can be obtained from the equation: $\sigma_{ext} = \sigma_{abs} + \sigma_{sca}$. The ratio of σ_{abs} to σ_{ext} at 800 nm was calculated to be 0.96 for the Au nanohexapod, which was roughly on the same order as what (0.91) was obtained experimentally from PA and UV-vis measurements. It is worth noting that this ratio was larger than those calculated using DDA method for both Au nanocages (0.82) with an outer edge length of 45.0 nm and Au nanorods (0.85) of 44.0 nm in length and 19.8 nm in width, but comparable to that (0.94) of Au nanocages with an outer edge length of 32.0 nm.[30]

Comparison of Photothermal Conversion *In Vitro*

We compared the photothermal conversion efficiencies of different types of Au nanostructures by measuring the temperature rise for their aqueous suspensions upon laser irradiation. Briefly, aqueous suspensions (100 μL) were placed in a single well of a 96-well plate and the radiation was delivered using a diode laser centered at 808 nm from the top at a density of 0.8 W/cm^2. A NIR camera was placed about 25 cm above the solution, and images were recorded at an interval of 15 s. The images were analyzed using the IR Flash software to obtain the average temperature of the suspension. As shown in Figure 2A, the suspension of Au nanohexapods (0.72 nM in particle concentration, with an extinction of 4.0 at 805 nm) showed a rapid increase in temperature during the first 3 min and eventually reached a plateau with a total temperature increase of 36.5 °C. The rate of temperature rise and the final temperature were proportional to the particle concentration; typically a slower and smaller increase was observed for a lower concentration of Au nanohexapods.

For the purpose of comparison, the extinction intensities of different samples were adjusted to 1.0 at 805 nm. As shown in Figure 2B, these three different types of Au nanostructures had a more or less similar efficiency for photothermal conversion on the basis of the same extinction intensity. However, given their large differences in structure and morphology, their conversion efficiencies could be drastically different when normalized to the total mass of Au atoms (or both Au and Ag atoms for the Au nanocage due to its alloyed composition).[35] As determined by ICP-MS, the concentrations of Au (or Au plus Ag for nanocages) atoms for the nanostructures were 34.4 μg/mL for nanohexapods, 36.4 μg/mL for nanorods, and 9.6 μg/mL for nanocages (together with an additional 3.3 μg/mL Ag atoms). As such, the photothermal conversion efficiency per Au atom was highest for nanocages, followed by nanohexapods, and then nanorods. It is worth noting that the continuous-wave diode laser caused no change to the optical properties of all three Au nanostructures, indicating that they were stable under the irradiation conditions. In the absence of any Au nanostructures, the solution only increased in temperature by 0.5 °C after 5 min of constant irradiation under similar conditions (Figure 2B).

Comparison of Photothermal Stability

We further characterized the photothermal stability of the Au nanostructures under pulsed laser irradiation. In a typical study, 100 μL of aqueous suspensions of Au nanostructures were exposed to a pulsed laser (λ = 805 nm) at a power density ranging from 15 – 35 mW/cm^2 for 15 min. The UV-vis spectra were taken to assess the stability. As shown in Figure S4, Au nanorods started to melt at 15 mW/cm^2, whereas Au nanohexapods and nanocages remained stable against laser irradiation under identical conditions without any observable LSPR shift. Both Au nanohexapods and nanocages started to melt at 25 mW/cm^2. Therefore, the Au nanohexapods and nanocages are much more photothermally stable than the Au nanorods.

Cell Toxicity *In Vitro*

The toxicity of these Au nanostructures was assessed using an assay based on 3-(4,5-dimethylthiazol-2-yl)-2,5-diphenyltetrazolium bromide (MTT), which involves the use of mitochondrial functional activity as an indicator. Figure 3A shows cell viabilities of MDA-MB-435 breast cancer cells after incubation for 48 h with the as-prepared Au nanostructures at different concentrations ranging from 1.56 to 200 μg/mL of Au atoms. For the CTAB-coated Au nanorods, they displayed significant cytotoxicity at concentrations higher than 3 μg/mL, with a half maximal inhibitory concentration (IC_{50}) of 10 μg/mL, indicating that they were highly toxic due to the presence of CTAB. When the CTAB was replaced by PEG (Mw ≈ 5,000), the observed cytotoxicity disappeared for samples with roughly the same concentrations (Figure 3B), similar to what was observed by other groups.[23] For PVP-coated Au nanocages, they also showed observable cytotoxicity at high concentrations, with a 20% loss of cell viability at 200 μg/mL (Figure 3A). The toxicity of Au nanocages was most likely due to the presence of Ag atoms in the alloyed structure and subsequent release of Ag^+ ions from Au nanocages during incubation.[35] After coating with PEG, the toxicity of Au nanocages was also substantially reduced (Figure 3B). Importantly, no significant cell toxicity was observed for either as-prepared or PEGylated Au nanohexapods at all concentrations we tested. This could be attributed to their pure Au composition, as well as the absence of a toxic surface capping ligand.

Cell Uptake *In Vitro*

Efficient cell entry is a prerequisite for Au nanostructures to function as photothermal transducers or diagnostic agents. It is important to understand how the different geometries of these Au nanostructures will impact their uptake by cells. The cell uptake was assessed with MDA-MB-435 cells cultured on glass cover slips and placed either in the upright or inverted configuration (with the cells facing the bottom of the cell culture plate).[36] The intracellular Au content was measured using ICP-MS following incubation for different periods of time. It is known that different surface chemistries (*i.e.*, capping ligands) will lead to variation in nanostructure uptake.[37–39] Therefore, we used PEGylated Au nanostructures for the cell uptake study to eliminate such an effect. As shown in Figure 4A for the upright configuration, the cell uptake of Au nanostructures was dependent on their geometries. The uptake of PEGylated Au nanorods was lower than that of PEGylated Au nanohexapods, while PEGylated Au nanocages had an intermediate uptake value. At 12 h after incubation, the cell uptake of PEGylated Au nanohexapods by MDA-MB-435 cells was 3.2 and 1.2 times that of PEGylated Au nanorods and PEGylated Au nanocages, respectively. This result indicates that the branched morphology of Au nanohexapods might have a higher probability to enter the cell in comparison with the rod- or cube-like morphology. Similar trends were also observed for the inverted configuration, where the sedimentation factor was eliminated.[36] The cell uptake was generally lower for cells in the inverted configuration than in the upright configuration, especially for Au nanocages due to the relatively larger mass for individual particles as well as the lower surface-to-volume ratio. Cellular uptake of PEGylated Au nanohexapods was 3.0 and 1.5 times that of PEGylated Au nanorods and PEGylated Au nanocages, respectively (Figure 4B).

Biodistributions

We next used an *in vivo* tumor model based on the MDA-MB-435 cell line to compare the biodistributions of these PEGylated Au nanostructures in blood and tissues after intravenous administration and their passive targeting efficiencies. PEG has been widely used to prevent or minimize absorption of serum proteins from the blood and thus increase the blood circulation time of nanostructures. The tumors were generated through subcutaneous injection of MDA-MB-435 cells in the right flanks of athymic mice. After the tumors had reached a proper size, the PEGylated Au nanostructures (100 μL, 4 nM in particle

concentration) were injected through the tail vein and the Au content contained in the blood and tissue samples were measured using ICP-MS at 6 h, 24 h, and 7 days post injection (p.i.). As shown in Figure 5 for the PEGylated Au nanohexapods, approximately 6.5±1.3 %ID/g (expressed relative to injected dose per gram tissue or blood) and 7.2±1.2 %ID/g of the injected particles were found in the tumor at 6 h and 24 h post-injection, respectively, suggesting significant accumulation in tumors due to the enhanced permeability and retention (EPR) effect in tumors with leaky vasculatures. The remaining PEGylated Au nanohexapods were taken up predominantly by the liver and to a lesser extent by the spleen related to the RES. Besides the liver and spleen, other organs with detectable Au levels were heart and lung, and to a less extent kidney. The mice injected with the PEGylated Au nanorods showed similar blood retention and accumulation (7.0±2.3 %ID/g at 6 h and 8.4±2.2 %ID/g at 24 h) in tumors. Both values were higher than the PEGylated Au nanocages (2.4±1.2 %ID/g at 6 h and 2.6±0.8 %ID/g at 24 h). On the other hand, different from PEGylated nanohexapods and nanocages, PEGylated Au nanorods showed a shift in distribution towards the spleen. At 7 days p.i., (Figure 5C), the levels of Au in the liver and spleen remained constant relative to those at 24 h. Interestingly, the concentrations of Au in the kidney and the blood pool organs (heart, lung, and blood) slightly decreased over time, indicating possible clearance of these Au nanostructures through the renal system. More importantly, the tumor accumulations of all these Au nanostructures did not show significant changes during the 7-day period of study, indicating stable residence in tumor. This feature might be advantageous for repeated or long term photothermal treatment. These results confirmed that the shape or morphology of nanostructures could influence their blood circulation and biodistributions. It should be pointed out that the dimensions of the Au nanostructures were different although the thicknesses of PEG coatings were roughly the same. Furthermore, our preliminary *in vivo* toxicity evaluation *via* hematoxylin and eosin staining did not show any observable adverse effect (Figure S5), indicating the *in vivo* biocompatibility of all these Au nanostructures.

In Vivo Photothermal Capability of Au Nanohexapods

We first quantitatively analyzed the photothermal conversion of the Au nanohexapods using a tumor model. In a typical study, either 40 μL of 1 nM Au nanohexapods (Figure S6, A1–A4) or 40 μL of saline (Figure S6, B1–B4) was administered intratumorally to tumor-bearing mice. Immediately after injection, the tumor regions were irradiated with a diode laser (808 nm) at a power density of 1.0 W/cm^2 for up to 5 min. The spot size was adjusted to cover the entire tumor area. For the mouse injected with Au nanohexapods, thermal images recorded at different time points indicate that the temperature of the tumor region quickly increased and then reached a plateau upon laser irradiation. As shown in Figure S6C, the temperature could easily reach a level (ΔT = 23.1 °C) capable of inducing hyperthermia to kill cancer cells.[17] In comparison, for the control mouse injected with saline, the temperature recorded from the tumor region was still in the homeostatically tolerable region, with ΔT = 4.2 °C. This result indicates that cell destruction will only result when Au hexapods and laser irradiation are both involved.

Comparison of Photothermal Treatment *In Vivo*

We further compared the photothermal cancer treatment efficacies of these PEGylated Au nanostructures in a bilateral MDA-MB-435 tumor model following intravenous administration. Tumor-bearing mice were administered intravenously with either 200 μL of the PEGylated Au nanostructures or 200 μL of saline, respectively (n = 3 per group). At 3 days post injection, the tumor on the left rear flank of each mouse was irradiated with a diode laser (808 nm) at a power density of 1.2 W/cm^2 for 10 min. For the mouse injected with PEGylated Au nanostructures, the temperature of the tumor region quickly increased and then reached a plateau upon laser irradiation, as compared with the mice injected with

saline (Figure 6A). The images were analyzed using the IR Flash software to obtain the average temperature of the suspension (Figure 6B). When compared with the PEGylated nanorods (53.0±0.5 °C) and nanocages (48.7±3.5 °C), PEGylated nanohexapods showed the highest (55.7±2.4 °C) photothermal conversion efficiency *in vivo*, owing to their highest tumor uptake and photothermal conversion efficiency per Au atom.

We next evaluated the effects of photothermal treatment by observing the tumor metabolism with ^{18}F-FDG PET/CT. Following intravenous administration of the various types of PEGylated Au nanostructures or saline, ^{18}F-FDG PET/CT imaging was performed before and 24 h after laser treatment. As shown in Figure 7A, the ^{18}F-FDG uptake was significantly reduced in the irradiated tumors in contrast to the contralateral non-irradiated tumors. Quantitative analysis showed substantial decrease of tumor standardized uptake values (SUVs) after the treatment for all the Au nanostructures while the non-irradiated tumors showed constant metabolism during the study (Figure 7B). More importantly, the irradiation/non-irradiation tumor SUV ratios demonstrated approximately 90% reduction of tumor metabolism in mice treated with nanohexapods or nanorods and 80% decrease in mice treated with nanocages, indicating almost complete destruction of tumor glycolic activity after the photothermal treatment (Figure 7C). Further, four days after the treatment, no visible tumors were observed in any of the treated mice.

The results indicate that all these PEGylated Au nanostructures could serve as effective transducers for photothermal treatment of cancer. Although there was no significant difference in treatment response from photothermal therapy as determined by ^{18}F-FDG uptake among the three Au nanostructures under the experimental conditions used in the present work, nanohexapods did cause a higher rise in temperature than nanorods or nanocages. Taken together, it is reasonable to expect that the combined high photothermal efficiency, low cytotoxicity, and substantial accumulation in tumor make Au nanohexapods a candidate photothermal transducer for further *in vivo* therapeutic evaluation. However, there is still a long way to go before the nanohexapods and other types of Au nanostructures can be translated into clinical practice. More efforts need to be devoted to further improve the pharmacokinetics, targeting efficiency, and longitudinal toxicity.

CONCLUSIONS

In summary, we have evaluated the potential use of Au nanohexapods for applications in photothermal cancer treatment. Our comparison studies with Au nanohexapods, nanorods, and nanocages indicate that all these Au nanostructures could absorb and convert NIR light into heat. Au nanohexapods exhibited the highest cellular uptake and the lowest cytotoxicity *in vitro* for both the as-prepared and PEGylated samples. The PEGylated Au nanohexapods also showed the significant blood circulation and tumor accumulation after intravenous injection. More importantly, the nanohexapods could significantly decrease the tumor metabolic activity following photothermal treatment after systemic administration. Combined together, it can be concluded that Au nanohexapods are promising as both optical therapeutic and diagnostic agents for a range of biomedical applications.

MATERIALS AND METHODS

Chemicals and Reagents

Poly(ethylene glycol) monomethyl ether thiol (mPEG-SH, Mw ≈ 5,000) was purchased from Laysan Bio (Arab, AL). All other chemicals or reagents, including cetyltrimethylammonium bromide (CTAB), dimethylformamide (DMF), chloroauric acid ($HAuCl_4$), indocyanine green (ICG), and (3-(4,5-dimethylthiazol-2-yl)-2,5-

diphenyltetrazolium bromide (MTT), were obtained from Sigma-Aldrich (St. Louis, MO). All chemicals were used as received.

Preparation and Characterization of Au Nanohexapods

The nanohexapods were prepared following our previously reported protocol with minor modifications.[28] In a typical synthesis, 0.2 mL of an aqueous suspension of the Au octahedral seeds was mixed with 4.8 mL ultrapurified H_2O (Millipore, Billerica, MA). At the same time, 2 mL DMF and 1 mL ultrapurified H_2O were mixed, heated to 120 °C for 10 min, and then cooled down to room temperature. 1 mL of this DMF/H_2O mixture was then added to the 5 mL suspension of Au octahedral seeds, followed by 10 μL of $HAuCl_4$ solution in DMF (9.42 mM) under stirring. The color of the solution changed from pink-red to blue. The $HAuCl_4$ solution in DMF was added every 15 min (10 μL each time) until the extinction peak of the reaction solution shifted to 805 nm. The product was collected by centrifugation at 10,000 rpm for 12 min and washed with water twice. The product was finally re-dispersed in water.

Synthesis of Au Nanocages

The nanocages were prepared using a galvanic replacement reaction between silver nanocubes and $HAuCl_4$ in an aqueous solution by following our previously published protocol.[34] The as-obtained nanocages was purified by centrifugation at 10,000 rpm for 10 min and washed twice with water. The product was finally re-dispersed in water.

Synthesis of Au Nanorods

The nanorods were synthesized using a seed-mediated method that involved the addition of a suspension of Au spherical seeds to a growth solution in the presence of CTAB as a capping agent.[25] The as-obtained nanorods was purified by centrifugation at 8,000 rpm for 15 min and washed once with water. The product was finally re-dispersed in water.

Measurement of Absorption Cross Section by PA Imaging

We used a dark-field illumination PA imaging system for the measurement.[40] A tunable Ti:sapphire laser (tuned to 805 nm, LT-2211A, Lotis TII, Minsk, Belarus) pumped by a Q-switched Nd:YAG laser (LS-2137, Lotis TII) was used for excitation at a pulse duration < 15-ns and a pulse repetition rate of 10 Hz. To protect the nanohexapods from melting/deformation or the ICG molecules from photobleaching, Tygon tubes were embedded in optically scattering medium, and the tubes were then filled with aqueous suspensions of the nanohexapods or aqueous solutions of ICG at different concentrations. When the solution was illuminated by laser, PA waves were generated through thermoelastic expansion due to optical absorption. A 5-MHz central frequency, spherically focused ultrasonic transducer (V308, Panametrics-NDT, Waltham, MA) was used to collect the PA signals. The signal was amplified by a low-noise amplifier (5072PR, Panametrics-NDT) and recorded using a digital oscilloscope (TDS5054, Tektronix, Beaverton, OR). A photodiode (SM05PD1A, Thorlabs, Newton, NJ) was used to compensate for the energy instability of laser pulses. The transducer was located inside a water container.

Conjugation of PEG with Au Nanostructures

Typically, 10 mL of ~1.0 nM Au nanohexapods (or nanocages) in ultra-purified H_2O was added to 5.0 mg of mPEG-SH (each Au nanoparticle corresponded to roughly 10^5 PEG molecules) and incubated overnight at room temperature. The excess mPEG-SH was removed by centrifugation at 10,000 rpm for 12 min (10,000 rpm for 10 min for Au nanocages) and washed three times with ultra-purified H_2O to obtain PEGylated Au nanohexapods (or PEGylated Au nanocages). Conjugation of PEG with CTAB-stabilized Au

nanorods was carried out using a similar procedure and purified by centrifugation at 8,000 rpm for 15 min. Considering the strong interaction of CTAB with Au nanorods, the PEGylation was repeated three times for each sample.

Photothermal Study

Aqueous suspensions of Au nanostructures (100 μL, at various particle concentrations) were placed in a single well of 96-well plate, and irradiated with a diode laser (λ=808 nm) from the top at a density of 0.8 W/cm^2. A NIR camera (ICI7320, Infrared Camera Inc., Beaumont, TX) was placed on top of the suspension, and thermographs were recorded by the NIR camera at an interval of five seconds. The thermographs were analyzed using IR Flash software (Infrared Camera Inc., version 2.10) to obtain the average temperature of the suspension at each time point.

In Vitro Photothermal Stability

Aqueous suspensions of Au nanostructures (0.1–0.2 nM, 100 μL) were placed in a cap of a 1.5-mL eppendorf centrifuge tube. The suspensions were irradiated with a pulsed laser (λ=805 nm) from the top at a density ranging from 15–35 mW/cm^2 for 15 min, and then the UV-vis spectra were recorded. A tunable Ti:sapphire laser (730–850 nm, LT-2211A, LOTIS TII, with pulse width <15 ns and a pulse repetition rate of 10 Hz) pumped by a Q-switched Nd:YAG (LS- 2137/2, LOTIS TII) was used for irradiation.

Cell Culture

MDA-MB-435 cell line was obtained from the American Type Culture Collection (ATCC, Manassas, VA). The cells were cultured in MEM medium, supplemented with 5% fetal bovine serum, penicillin (10^4 IU)/streptomycin (10 mg/mL), 2 mM L-glutamine, 1 mM sodium pyruvate, 1 mM non-essential amino acids, and 20 mM vitamins for MEM at 37 °C using a humidified 5% CO_2 incubator.

In Vitro Cell Uptake Studies Using ICP-MS

In the upright configuration, MDA-MB-435 cells were seeded in 24-well plates at a density of 1×10^5 cells/well and incubated overnight. The cells were washed with PBS and incubated with the culture medium containing the PEGylated Au nanostructures. After different intervals of time, the cells were washed three times with cold PBS, treated with 0.2 mL of trypsin solution (containing 0.25% EDTA), and counted with a hematocytometer. The cell pellets were freeze-dried and 400 μL aqua regia was then added to completely digest the cells and dissolve the Au nanostructures. The amount of Au was measured by Elan DRC II ICP-MS (Perkin Elmer, Waltham, MA). Quantification was carried out by external five-point calibration with internal standard correction. The amount of Au was finally normalized to the cell number. In the inverted configuration (with the cells facing the bottom of the well), MDA-MB-435 cells were seeded on round coverslips (diameter = 25 mm, VWR, Radnor, PA) until ~80% confluence was reached. The coverslips were washed with PBS five times and suspended from above by gluing a small block of rubber on the back side of the coverslip and a syringe needle to the inner side of the cover of a 6-well culture plate.[35] The cells were incubated with the culture medium containing the PEGylated Au nanostructures. At different intervals of time, the cells were washed three times with cold PBS, treated with 0.4 mL of trypsin solution (containing 0.25% EDTA) and counted with a hematocytometer. The Au content was analyzed using ICP-MS as described above.

In Vitro Cell Growth Inhibition Assay

MDA-MB-435 cells were seeded in 96-well plates at a density of 5×10^3 cells per well in 100 μL of complete MEM medium, and incubated at 37 °C in 5% CO_2 humidified

atmosphere for 24 h. The culture medium was then replaced with 100 μL of freshly prepared culture medium containing the as-prepared Au nanostructures or the PEGylated Au nanostructures at different concentrations from 1.56 to 200 μg/mL of Au atoms. The cells were further incubated for 48 h, and then 25 μL of MTT stock solution (5 mg/mL in PBS) was added to each well to achieve a final concentration of 1 mg/mL, with the exception of the well labeled as blank to which 25 μL of PBS was added. After incubation for another 2 h, 100 μL of extraction buffer (20% SDS in 50% DMF, pH 4.7, prepared at 37 °C) was added to the wells and incubated at 37 °C for another 4 h. The absorbance was measured at 570 nm using an Infinite F200 multimode reader (Tecan, Switzerland). Cell viability was normalized to that of MDA-MB-435 cells cultured in the complete culture medium.

In Vivo Biodistribution Analysis

Athymic Nude-Foxn1nu nude mice, aged 5–6 weeks, were obtained from Harlan Laboratories (Indianapolis, IN). The MDA-MB-435 tumor model was generated by subcutaneous injection of 5×10^6 cells in 30–40 μL PBS into the right rear flanks. Animals used in biodistribution studies had a tumor volume of 200–300 mm^3 for 6 and 24 h studies and 100–200 mm^3 for 7 days experiments. The tumor-bearing mice were randomly divided into six groups (n = 3 per group). The mice were injected intravenously with 100 μL of PEGylated Au nanostructures (4 nM). At 6 h, 24 h, and 7 days post injection, animals were sacrificed and the tissues were taken out, washed, weighed, and then freeze-dried. The tissue sample was digested with 8 mL of aqua regia in a 20 mL glass vials at boiling temperature. The solution was evaporated and suspended in aqueous solution containing 0.5% HCl and 1.5% HNO_3. The suspension was centrifuged at a speed of 3,000 rpm to remove any undigested debris prior to ICP-MS measurement. The analysis of Au content was performed using ICP-MS as described above.

Evaluation of *In Vivo* Photothermal Conversion Following Intratumoral Injection

Animals were anesthetized with 2% isoflurane (ISoFlo, Abott Laboratories) in 100% oxygen, placed in a prone position on a table, and injected with 40 μL of an aqueous suspension of PEGylated Au nanohexapods (1 nM) or saline intratumorally. The entire region of the tumor was then exposed to a diode laser (808 nm) at a power density of 1.0 W/cm^2. During irradiation, thermographs were taken using a NIR camera as described above.

In Vivo Photothermal Treatment Following Intravenous Injection

MDA-MB-435 tumors were grown in both rear flanks of athymic Nude-Foxn1nu nude mice in the same way described above (one tumor for irradiation, one for control). Mice were injected intravenously with 200 μL of PEGylated Au nanostructures or saline (n = 3 per group, Au atom mass ≈ 0.8 mg per mouse). At 72 h post injection, animals were anesthetized with 2% isoflurane (ISoFlo, Abott Laboratories) in 100% oxygen and placed in a prone position on a table. The entire region of the left-side tumor was then exposed to a diode laser (808 nm) at a power density of 1.2 W/cm^2. During irradiation, thermographs were taken using a NIR camera as described above. 4 days after irradiation, mice were sacrificed and irradiated sites were interrogated for the presence of tumors.

Positron Emission Tomography/Computed Tomography (PET/CT) Imaging

The photothermal treatment effect on tumor metabolism was assessed by ^{18}F-flourodeoxyglucose (^{18}F-FDG) PET/CT before the injection of various gold nanostructures and 24 h post treatment. Athymic nude-foxn1nu nude mice bearing MDA-MB-435 tumors in each rear flank (one irradiated and one control per mouse) were fasted overnight, anesthetized with isoflurane (2% in 100% O_2), and injected with 3.66 – 4.59 MBq ^{18}F-FDG in 100 μL saline acquired from the Washington University cyclotron facility *via* the tail

vein. A 10 minute static scan was performed one hour after ^{18}F-FDG injection with either an Inveon microPET/CT Scanner (Siemens, Munich, Germany) or a Focus 220 PET Scanner (Concorde Microsystems, Knoxville, TN). The microPET images were corrected for attenuation, scatter, normalization, and camera dead time and co-registered with microCT images. All of the PET scanners were cross-calibrated periodically. The microPET images were reconstructed with the maximum a posteriori (MAP) algorithm and analyzed by Inveon Research Workplace. The tumor uptake of ^{18}F-FDG was calculated in terms of the standardized uptake value (SUV) in three-dimensional regions of interest (ROIs). In general, SUV is defined as the tissue concentration of radiotracer divided by the activity injected per body weight and is calculated according to the following equation:

$$(\text{Activity}_{\text{tumor}}/\text{Volume}_{\text{tumor}}) * (\text{Weight}_{\text{animal}})/(\text{Activity}_{\text{injected}} * (1/2)\text{^}(\text{n}_{\text{half lives}}))$$

All the SUV data were not corrected for partial volume effect.[41]

In Vivo Toxicity

C57BL/6 mice weighing 20–25 g (Charles River Laboratory, Wilmington, MA) were injected intravenously with 100 μL of PEGylated Au nanostructures or saline (n = 3 per group, Au atom mass ≈ 0.4 mg per mouse). At 7 days post injection, animals were sacrificed and the tissues were excised. The excised tissues were embedded in paraffin blocks, sectioned into 7-mm slices, and stained with hematoxylin and eosin (Sigma–Aldrich) to assess tissue and cellular morphology.

Instrumentations

The UV-Vis extinction spectra were recorded using a Cary 50 spectrometer (Varian, Palo Alto, CA). Prior to their use, the Au nanostructures were characterized using a Tecnai G^2 Spirit transmission electron microscope (TEM) operated at 120 kV (FEI, Hillsboro, OR).

Supplementary Material

Refer to Web version on PubMed Central for supplementary material.

Acknowledgments

This work was supported by a grant from the NCI (R01 CA138527). M. Li was an REU student from Duke University and he was supported by the NSF NNIN program. We thank the Division of Comparative Medicine Research Animal Diagnostic Laboratory at Washington University School of Medicine for histology analysis.

References

1. Kennedy LC, Bickford LR, Lewinski NA, Coughlin AJ, Hu Y, Day ES, West JL, Drezek RA. A New Era for Cancer Treatment: Gold-Nanoparticle-Mediated Thermal Therapies. Small. 2011; 7:169–183. [PubMed: 21213377]
2. Frangioni JV. *In Vivo* Near-Infrared Fluorescence Imaging. Curr Opin Chem Biol. 2003; 7:626–634. [PubMed: 14580568]
3. Barone PW, Baik S, Heller DA, Strano MS. Near-Infrared Optical Sensors Based on Single-Walled Carbon Nanotubes. Nat Mater. 2005; 4:86–U16. [PubMed: 15592477]
4. Jain PK, Huang X, El-Sayed IH, El-Sayed MA. Noble Metals on the Nanoscale: Optical and Photothermal Properties and Some Applications in Imaging, Sensing, Biology, and Medicine. Acc Chem Res. 2008; 41:1578–1586. [PubMed: 18447366]

5. O'Neal DP, Hirsch LR, Halas NJ, Payne JD, West JL. Photo-Thermal Tumor Ablation in Mice Using Near Infrared-Absorbing Nanoparticles. Cancer Lett. 2004; 209:171–176. [PubMed: 15159019]
6. Zheng XH, Zhou FF, Wu BY, Chen WR, Xing D. Enhanced Tumor Treatment Using Biofunctional Indocyanine Green-Containing Nanostructure by Intratumoral or Intravenous Injection. Mol Pharmaceut. 2012; 9:514–522.
7. Li D, Huang J, Kaner RB. Polyaniline Nanofibers: A Unique Polymer Nanostructure for Versatile Applications. Acc Chem Res. 2009; 42:135–145. [PubMed: 18986177]
8. Hu M, Chen J, Li ZY, Au L, Hartland GV, Li X, Marquez M, Xia Y. Gold Nanostructures: Engineering Their Plasmonic Properties for Biomedical Applications. Chem Soc Rev. 2006; 35:1084–1094. [PubMed: 17057837]
9. Huang XQ, Tang SH, Mu XL, Dai Y, Chen GX, Zhou ZY, Ruan FX, Yang ZL, Zheng NF. Freestanding Palladium Nanosheets with Plasmonic and Catalytic Properties. Nat Nanotechnol. 2011; 6:28–32. [PubMed: 21131956]
10. Moon HK, Lee SH, Choi HC. *In Vivo* Near-Infrared Mediated Tumor Destruction by Photothermal Effect of Carbon Nanotubes. ACS Nano. 2009; 3:3707–3713. [PubMed: 19877694]
11. Kim J, Galanzha EI, Shashkov EV, Moon H, Zharov VP. Golden Carbon Nanotubes as Multimodal Photoacoustic and Photothermal High-Contrast Molecular Agents. Nat Nanotechnol. 2009; 4:688–694. [PubMed: 19809462]
12. Li M, Yang X, Ren J, Qu K, Qu X. Using Graphene Oxide High Near-Infrared Absorbance for Photothermal Treatment of Alzheimer's Disease. Adv Mater. 2012; 24:1722–1728. [PubMed: 22407491]
13. Yang K, Zhang SA, Zhang GX, Sun XM, Lee ST, Liu ZA. Graphene in Mice: Ultrahigh *In Vivo* Tumor Uptake and Efficient Photothermal Therapy. Nano Lett. 2010; 10:3318–3323. [PubMed: 20684528]
14. Sepulveda B, Angelome PC, Lechuga LM, Liz-Marzan LM. LSPR-Based Nanobiosensors. Nano Today. 2009; 4:244–251.
15. Nam J, Won N, Jin H, Chung H, Kim S. pH-Induced Aggregation of Gold Nanoparticles for Photothermal Cancer Therapy. J Am Chem Soc. 2009; 131:13639–13645. [PubMed: 19772360]
16. Bardhan R, Lal S, Joshi A, Halas NJ. Theranostic Nanoshells: From Probe Design to Imaging and Treatment of Cancer. Acc Chem Res. 2011; 44:936–946. [PubMed: 21612199]
17. Chen J, Glaus C, Laforest R, Zhang Q, Yang M, Gidding M, Welch MJ, Xia Y. Gold Nanocages as Photothermal Transducers for Cancer Treatment. Small. 2010; 6:811–817. [PubMed: 20225187]
18. Huang XH, El-Sayed IH, Qian W, El-Sayed MA. Cancer Cell Imaging and Photothermal Therapy in the Near-Infrared Region by Using Gold Nanorods. J Am Chem Soc. 2006; 128:2115–2120. [PubMed: 16464114]
19. Ye EY, Win KY, Tan HR, Lin M, Teng CP, Mlayah A, Han MY. Plasmonic Gold Nanocrosses with Multidirectional Excitation and Strong Photothermal Effect. J Am Chem Soc. 2011; 133:8506–8509. [PubMed: 21563806]
20. Azzazy HME, Mansour MMH, Samir TM, Franco R. Gold Nanoparticles in the Clinical Laboratory: Principles of Preparation and Applications. Clin Chem Lab Med. 2012; 50:193–209. [PubMed: 21973106]
21. [accessed January 2013] Pilot Study of AuroLase Therapy in Refractory and/or Recurrent Tumors of the Head and Neck. http://clinicaltrials.gov/ct2/show/NCT00848042
22. Gad SC, Sharp KL, Montgomery C, Payne JD, Goodrich GP. Evaluation of the Toxicity of Intravenous Delivery of Auroshell Particles (Gold-Silica Nanoshells). Int J Toxicol. 201310.1177/1091581812465969
23. Grabinski C, Schaeublin N, Wijaya A, D'Couto H, Baxamusa SH, Hamad-Schifferli K, Hussain SM. Effect of Gold Nanorod Surface Chemistry on Cellular Response. ACS Nano. 2011; 5:2870–2879. [PubMed: 21405102]
24. Hao F, Nehl CL, Hafner JH, Nordlander P. Plasmon Resonances of a Gold Nanostar. Nano Lett. 2007; 7:729–732. [PubMed: 17279802]

25. Goodrich GP, Bao L, Gill-Sharp K, Sang KL, Wang J, Payne JD. Photothermal Therapy in a Murine Colon Cancer Model Using Near-Infrared Absorbing Gold Nanorods. J Biomed Opt. 2010; 15:018001. [PubMed: 20210487]
26. Van de Broek B, Devoogdt N, D'Hollander A, Gijs HL, Jans K, Lagae L, Muyldermans S, Maes G, Borghs G. Specific Cell Targeting with Nanobody Conjugated Branched Gold Nanoparticles for Photothermal Therapy. ACS Nano. 2011; 5:4319–4328. [PubMed: 21609027]
27. Hasan W, Stender CL, Lee MH, Nehl CL, Lee J, Odom TW. Tailoring the Structure of Nanopyramids for Optimal Heat Generation. Nano Lett. 2009; 9:1555–1558. [PubMed: 19271715]
28. Kim DY, Yu T, Cho EC, Ma Y, Park OO, Xia Y. Synthesis of Gold Nano-hexapods with Controllable Arm Lengths and Their Tunable Optical Properties. Angew Chem Int Edit. 2011; 50:7972–7972.
29. Kumar PS, Pastoriza-Santos I, Rodriguez-Gonzalez B, Garcia de Abajo FJ, Liz-Marzan LM. High-Yield Synthesis and Optical Response of Gold Nanostars. Nanotechnology. 2008; 19:015606. [PubMed: 21730541]
30. Cho EC, Kim C, Zhou F, Cobley CM, Song KH, Chen J, Li ZY, Wang LV, Xia Y. Measuring the Optical Absorption Cross Sections of Au-Ag Nanocages and Au Nanorods by Photoacoustic Imaging. J Phys Chem C. 2009; 113:9023–9028.
31. Optical Absorption of Indocyanine Green. http://omlc.ogi.edu/spectra/icg/index.html
32. Nikoobakht B, El-Sayed MA. Preparation and Growth Mechanism of Gold Nanorods (NRs) Using Seed-Mediated Growth Method. Chem Mater. 2003; 15:1957–1962.
33. Sau TK, Murphy CJ. Seeded High Yield Synthesis of Short Au Nanorods in Aqueous Solution. Langmuir. 2004; 20:6414–6420. [PubMed: 15248731]
34. Skrabalak SE, Au L, Li X, Xia Y. Facile Synthesis of Ag Nanocubes and Au Nanocages. Nat Protoc. 2007; 2:2182–2190. [PubMed: 17853874]
35. Zhang Q, Cobley CM, Zeng J, Wen LP, Chen J, Xia Y. Dissolving Ag from Au-Ag Alloy Nanoboxes with H_2O_2: A Method for Both Tailoring the Optical Properties and Measuring the H_2O_2 Concentration. J Phys Chem C. 2010; 114:6396–6400.
36. Cho EC, Zhang Q, Xia YN. The Effect of Sedimentation and Diffusion on Cellular Uptake of Gold Nanoparticles. Nat Nanotechnol. 2011; 6:385–391. [PubMed: 21516092]
37. Walkey CD, Olsen JB, Guo H, Emili A, Chan WCW. Nanoparticle Size and Surface Chemistry Determine Serum Protein Adsorption and Macrophage Uptake. J Am Chem Soc. 2012; 134:2139–2147. [PubMed: 22191645]
38. Nativo P, Prior IA, Brust M. Uptake and Intracellular Fate of Surface-Modified Gold Nanoparticles. ACS Nano. 2008; 2:1639–1644. [PubMed: 19206367]
39. Hauck TS, Ghazani AA, Chan WCW. Assessing the Effect of Surface Chemistry on Gold Nanorod Uptake, Toxicity, and Gene Expression in Mammalian Cells. Small. 2008; 4:153–159. [PubMed: 18081130]
40. Song KH, Wang LV. Deep Reflection-Mode Photoacoustic Imaging of Biological Tissue. J Biomed Opt. 2007; 12:060503. [PubMed: 18163798]
41. Wang Y, Liu Y, Luehmann H, Xia X, Brown P, Jarreau C, Welch M, Xia Y. Evaluating the Pharmacokinetics and *In Vivo* Cancer Targeting Capability of Au Nanocages by Positron Emission Tomography Imaging. ACS Nano. 2012; 6:5880–5888. [PubMed: 22690722]

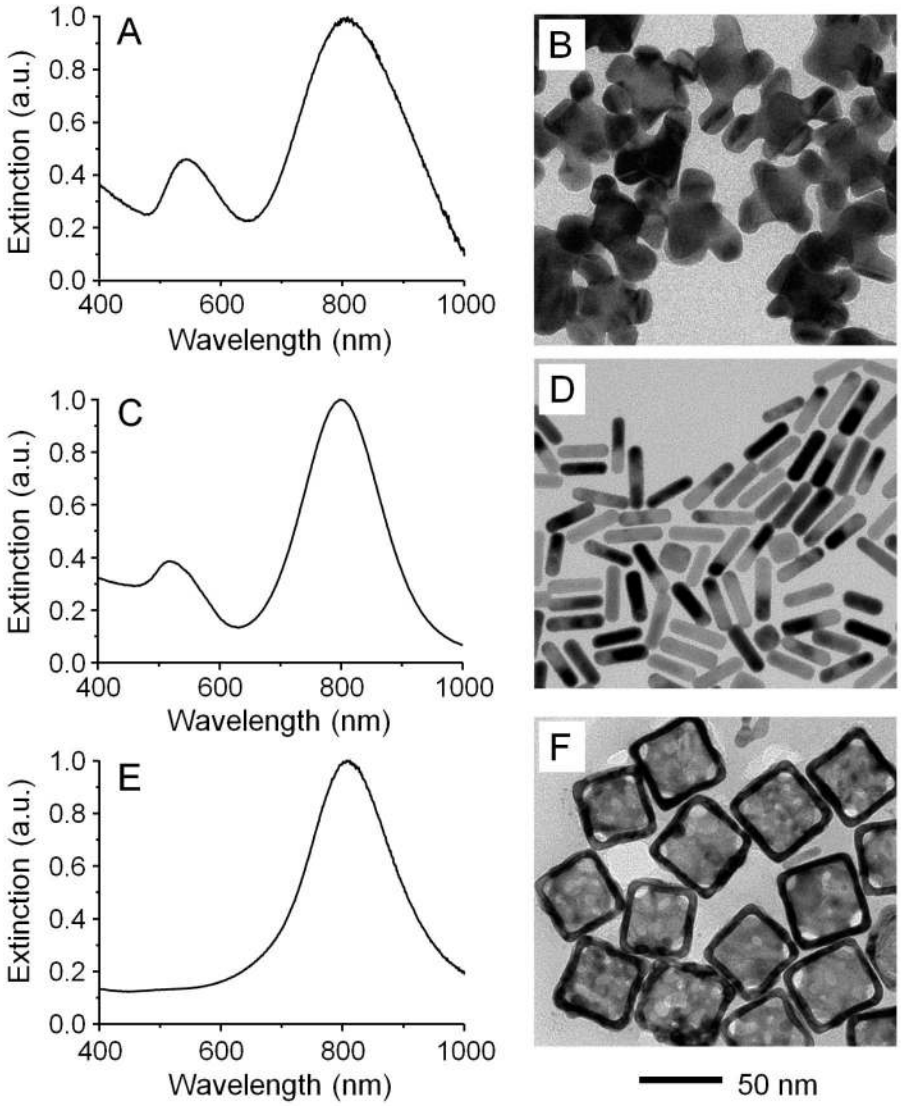

Figure 1.

UV-vis spectra taken from aqueous suspensions of (A) Au nanohexapods (0.18 nM in particle concentration or 34.4 μg/mL of Au atoms), (C) Au nanorods (1.4 nM in particle concentration or 36.4 μg/mL of Au atoms), and (E) Au nanocages (0.024 nM in particle concentration or 9.6 μg/mL of Au atoms and 3.3 μg/mL of Ag atoms). (B, D, F) TEM images of the corresponding Au nanostructures. The 50 nm scale bar applies to all images.

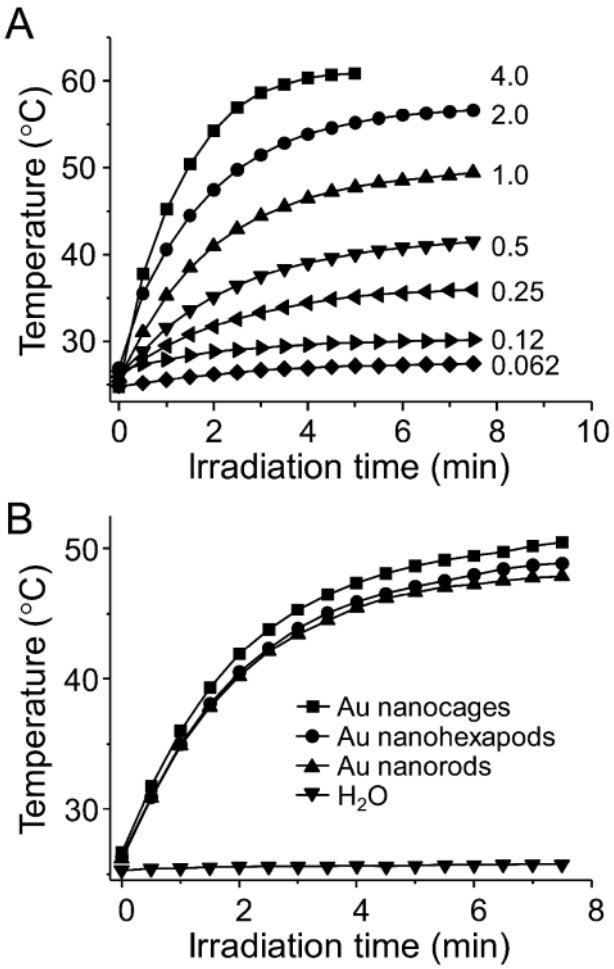

Figure 2.

(A) Plots of temperatures as a function of irradiation time for aqueous suspensions of Au nanohexapods with different extinction intensities (or particle concentrations) ranging from 0.062 (or 0.011 nM) to 4.0 (or 0.72 nM). The number next to the curve indicates extinction intensity of the suspension at 805 nm. (B) Plots of temperatures as a function of irradiation time for suspensions of Au nanohexapods, nanorods, and nanocages. For the purpose of comparison, the concentration of each suspension was adjusted to give an extinction intensity of 1.0 at 805 nm. The laser power density was 0.8 W/cm^2.

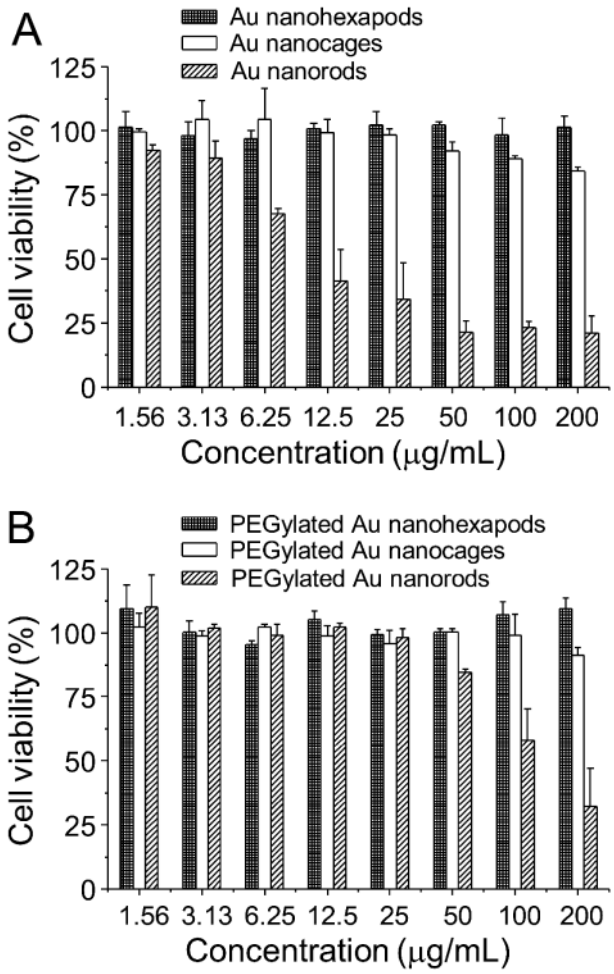

Figure 3.

(A) Cell viability of MDA-MB-435 cells after incubation with the as-synthesized Au nanohexapods, nanocages, and nanorods for 48 h. (B) Cell viability of MDA-MB-435 cells after incubation with the PEGylated Au nanohexapods, nanocages, and nanorods for 48 h. Error bars are standard errors with n = 6.

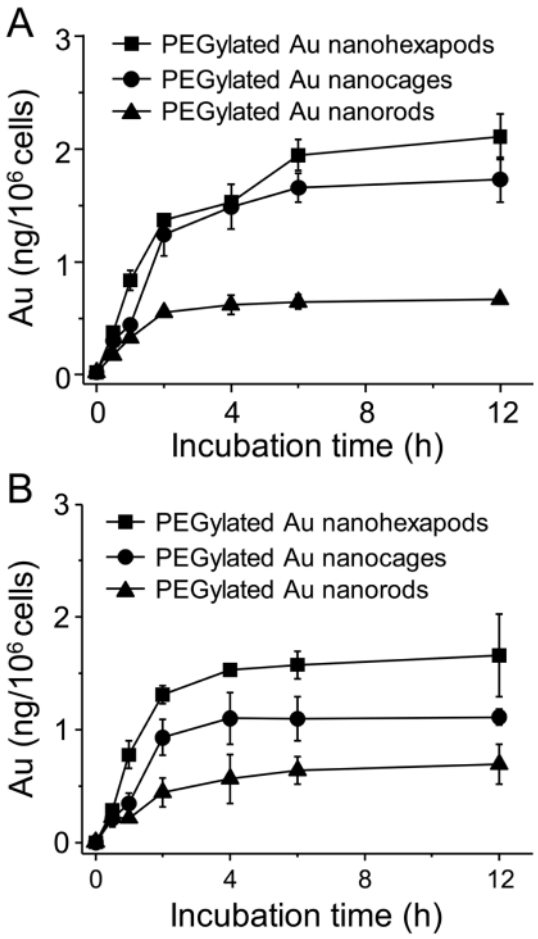

Figure 4.

Uptake of the PEGylated Au nanohexapods, nanocages, and nanorods by MDA-MB-435 cells after incubation for different periods of time. The cells were positioned in (A) upright configuration and (B) inverted configuration. The initial concentrations of Au atoms in the culture medium were 10 μg/mL for each sample of Au nanostructures. Error bars are standard errors with n = 4.

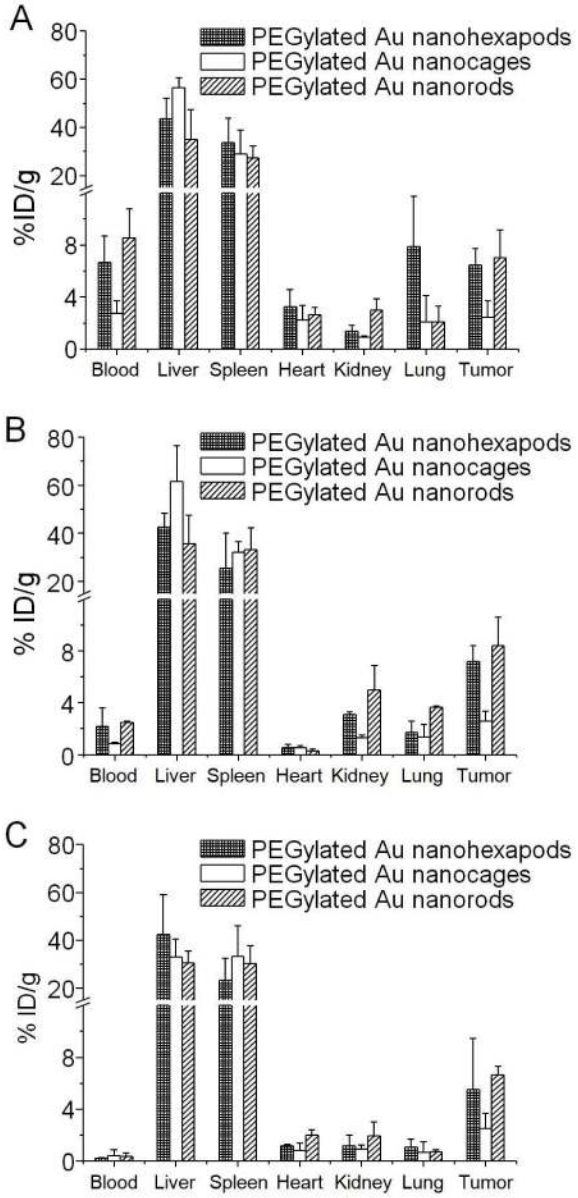

Figure 5.

In vivo biodistributions of the PEGylated Au nanohexapods, nanocages, and nanorods after they had been intravenously injected into tumor-bearing mice for (A) 6 h, (B) 24 h, and (C) 7 days. The amounts of Au in the tissues were analyzed by ICP-MS. Error bars are standard errors with n = 3.

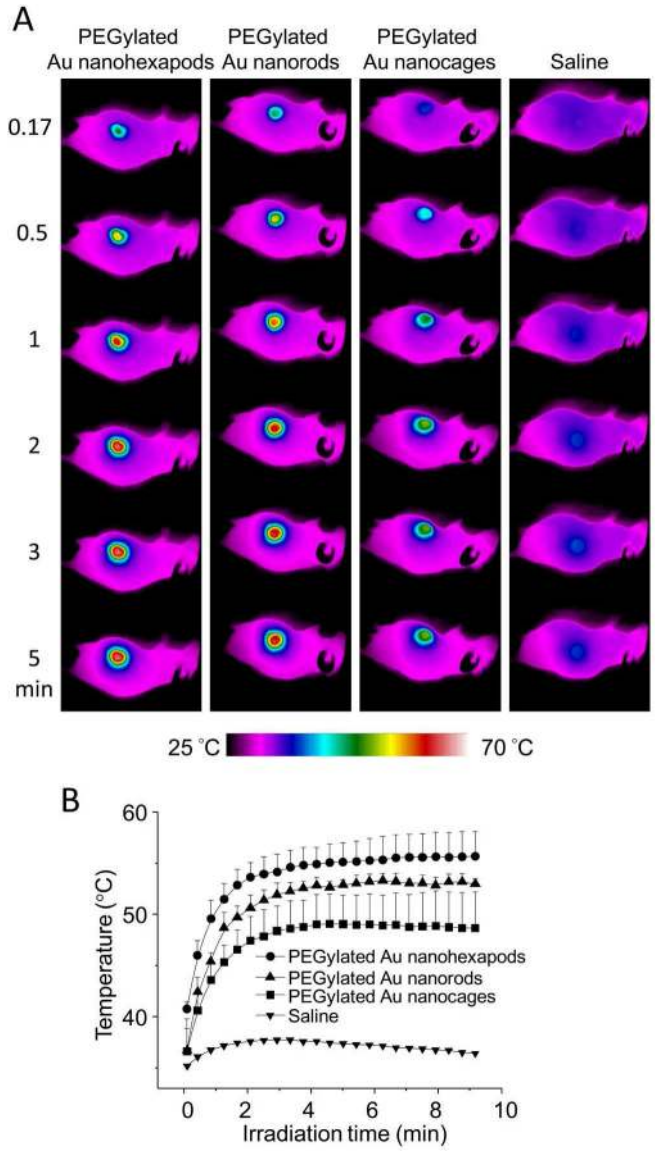

Figure 6.

A) Thermographs of tumor-bearing mice receiving photothermal treatment for different periods of time. The mice were intravenously administrated with aqueous suspensions of PEGylated nanohexapods, nanorods, nanocages, or saline. B) Plots of average temperature increase within the tumor region as a function of irradiation time. The laser power density was 1.2 W/cm^2. Error bars are standard errors with n = 3.

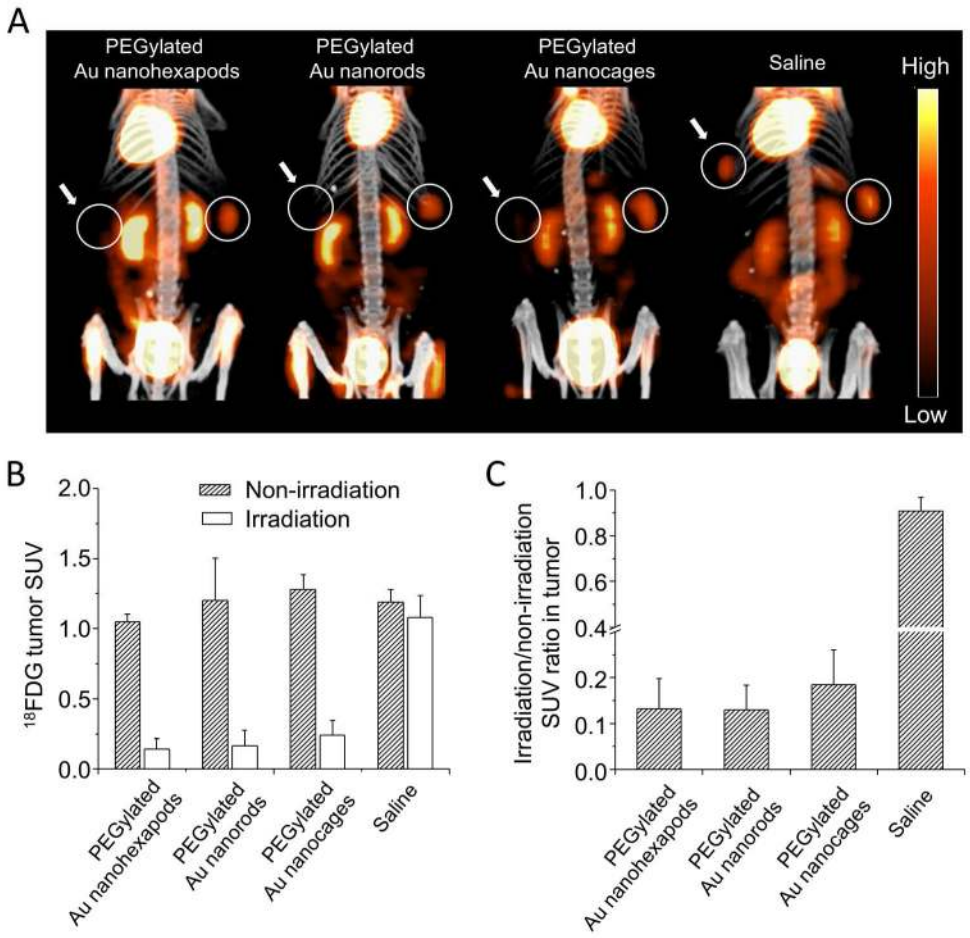

Figure 7.

A) ^{18}F-FDG PET/CT co-registered images of mice intravenously administrated with aqueous suspensions of PEGylated nanohexapods, nanorods, nanocages, or saline. Tumors were treated either with (solid circle + left arrow) or without (solid circle) laser irradiation. B) A plot showing ^{18}F-FDG standardized uptake values (SUV) in laser-treated tumor and non-treated tumor. C) A plot showing the ratios of laser-treated tumor to non-treated tumor ^{18}F-FDG SUV. Error bars are standard errors with n = 3.